Journal of Alloys and Compounds 505 (2010) 534–541

Contents lists available at ScienceDirect

Journal of Alloys and Compounds

journal homepage: www.elsevier.com/locate/jallcom

Phase transformation studies on YSZ doped with alumina. Part 2: Yttria segregation

Soroush Nazarpour[a,*], Carlos López-Gándara[a,b], Cyrus Zamani[a], Josep M. Fernández-Sanjuán[b], Francisco M. Ramos[b], Albert Cirera[a]

[a] MIND/IN2UB, Departament d'Electrònica, Universitat de Barcelona, Martí i Franquès 1, Barcelona 08028, Spain
[b] FAE—Francisco Albero S.A. Rafael Barradas 19, L'Hospitalet de Llobregat 08908, Spain

ARTICLE INFO

Article history:
Received 8 March 2010
Received in revised form 17 May 2010
Accepted 28 May 2010
Available online 11 June 2010

Keywords:
Yttria deficiency
YSZ
Alumina oversaturation
Segregation
Tetragonality
Oxygen sensor

ABSTRACT

Yttria and alumina segregations in annealed alumina-doped YSZ at 800 °C and 1000 °C for different annealing times were discussed. Segregation of yttria into the grain boundaries of YSZ was detected which leads to its deficiency in the YSZ grains. Low dopant concentration in YSZ grains may result in cubic and/or tetragonal to monoclinic phase transformation. Hence, variation of the mechanical and electrical properties of YSZ as a function of annealing temperature was studied. Finally, the material was studied as an oxygen sensor implemented in a real engine where it exposed to the exhaust gas for 50,000 h. Microstructural investigations show that these working conditions lead to the formation of monoclinic phase; cubic YSZ is fully removed whereas tetragonal phase is partially disappeared which confirms the proposed effect of yttria segregation upon the sensor lifetime. This study reveals the importance of considering the degradation of electrolyte material in the high temperature applications such as gas sensing.

1. Introduction

Pure (undoped) ZrO_2 ceramics exhibit a monoclinic (m) to tetragonal (t) phase transformation at 1170 °C and tetragonal to cubic phase transition at 2370 °C. Moreover, cubic to liquid phase transformation occurs at 2680 °C [1–3]. It is well known that a reversible athermal martensitic transformation from monoclinic to tetragonal occurs in pure zirconia during cooling, associated with a large shear strain due to a volume change of 5–10%. This transformation is destructive and leads to micro and macrocracks which could annihilate the ceramic and result in the formation of crumbled parts of pure zirconia. Dopants, such as Y_2O_3, are usually added to the sintered powder for improving the high temperature stability of tetragonal and cubic phases. Fig. 1 depicts to the ZrO_2–Y_2O_3 phase diagram together with T0-lines proposed by Yashima et al. [4]. Numerous phase diagrams correspond to YSZ could be found in the literature [5–7]. These phase diagrams represent the equilibrium phase diagram along with T0-lines for diffusionless transformations of cubic to tetragonal (c–t) and tetragonal to monoclinic (t–m). In fact, metastable equilibrium corresponds to the local minimum of the Gibbs energy function, while T0-line corresponds to the situation when the Gibbs energy of one phase is equal to the other one. Hence, T0-line does not correspond to a minimum of Gibbs energy for two-component system. T0-line in Fig. 1 represents the solubility of the yttria into tetragonal phase in non-equilibrium states.

Perpendicular dashed line in Fig. 1 indicates the yttria concentration in the samples and the main phases at different temperatures. As the diffusion of the cations at low temperatures is limited, it is impossible to attain the true phase transformation using conventional heat treatments. Additionally, monoclinic, tetragonal and cubic phases may undergo diffusionless phase transitions and cause as well considerable discrepancies among the proposed phase diagrams. It can be concluded from these diagrams that at higher temperatures, tetragonal YSZ converts to cubic phase. Solid solution of zirconia stabilized with 4.5 mol% yttria is an important solid electrolyte material, particularly in ceramic based gas sensing applications. In fact, doping of oxides stabilizes the high-temperature cubic and tetragonal phases at room temperature. Stabilizing the high temperature phases at room temperate results in an enhancement in the density of the oxygen vacancies and enrichment in the oxygen-ion conductivity. Higher ionic conductivity facilitates to exploit this stabilized zirconia as an electrolytic material [4,8]. Y-TZP is an O^{2-} ion-conducting material at temperatures above 300 °C. The conductivity requirement for the electrolyte determines the operating temperature of the gas sensors to be about 1000 °C. Hence, the stability and phase transformations of the YSZ electrolyte at 1000 °C are of great importance.

* Corresponding author. Tel.: +34 934039174.
E-mail address: nazarpour@ub.edu (S. Nazarpour).

0925-8388/$ – see front matter © 2010 Elsevier B.V. All rights reserved.
doi:10.1016/j.jallcom.2010.05.137

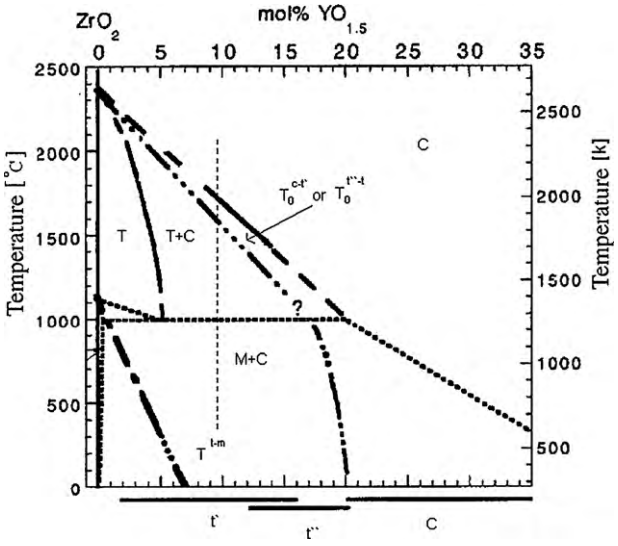

Fig. 1. Phase diagram of the YSZ. Phases illustrated in the figure are as follows: T, tetragonal; C, cubic and M, monoclinic.

An enhancement in mechanical properties with relatively constant ionic conductivity has been already reported after addition of alumina into YSZ [9]. However, oversaturation of alumina forms precipitates predominantly at grain boundaries [10] which scavenge the silicon rich second phase from grain boundaries. In one hand, scavenging the silicon phase from grain boundaries to triple point boundaries decreases the grain boundary resistance [11] due to diminishing their blocking effect. On the other hand, it could be expected that oversaturation of alumina introduces extra precipitates on the grain boundaries and increases the grain boundary resistance as a result of space charge layers around them [12]. The goal of this study on YSZ as electrolyte material in oxygen sensing application is to investigate the effect of high temperature exposure upon segregation of dopants (alumina and yttria). Segregation of dopants may introduce phase transformation inside the grain and at the grain boundaries of YSZ which directly affects the ionic conductivity and lifetime of the YSZ-based oxygen sensor.

2. Experimental

Specimens were made based on tape casting and multilayer planar ceramic technologies through sintering of 4.5 mol% Y_2O_3, 9.4 mol% Al_2O_3, and zirconia (balance), as electrolyte [13–16]. The microstructure was examined by scanning electron microscopy (SEM) (ESEM Quanta 200 FEI), transmission electron microscopy (TEM) (Hitachi 800MT, 300 kV) and high resolution transmission electron microscopy (HRTEM) (JEOL JEM 2100, 200 kV). Besides, nanoprobe energy dispersive spectroscopy (EDS) was conducted to investigate the segregation of dopants into the grain boundaries. Specimens for TEM observations were prepared via conventional preparation techniques, polishing, dimple grinding, and ion milling to obtain electron transparency.

All sensors were sintered at 1450 °C for 3 h. The crystalline structure was determined by X-ray diffraction (XRD) analysis in θ–2θ scan by means of a 4-circle X-ray diffractometer with Cu Kα radiation (MRD PHILIPS) (0.05° step size, 1 min scan time/step) and high accuracy XRD (Pananalytical) (0.005° step size, 3 min scan time/step). Measurements were done at various temperatures in order to investigate the effect of temperature upon the phase structure of YSZ electrolyte with respect to the variation of $c/(a\sqrt{2})$ ratio (tetragonality).

Additionally, Raman spectroscopy (Jobin Yvon T64000) was carried out to illustrate the structural properties of the as-produced and annealed samples.

Observations of the outer surface of samples by SEM allowed us both to determine their microstructure (mainly the grain size), and to accurately observe the indentation prints and the morphology of cracks. Vickers indentations were made on polished samples using a Galileo ISOSCAN hardness testing machine with a maximum load of 10 N held for 15 s. Each sample was tested for times with a spacing of about 2 mm.

Furthermore, a mixture of platinum and YSZ was deposited over YSZ by means of screen printing to serve as electrode [13–16]. To avoid any dependence on undesired parameters, electrodes and heating elements had identical dimensions, composition and fabrication method in all the designed sensors [13]. Impedance spectroscopy (using both Solarton SI-1260 frequency response analyzer and a Gamry Potentiostat PCI4/750) was implemented to compare the electrolyte resistance, heated from 450 °C to 950 °C, always exposed to air. Three cycles of measurements were carried out in order to identify the effect of thermal cycles on the resistance of electrolyte. Afterwards, a series of YSZ specimens were annealed at 800 °C and 1000 °C for 1 h, 6 h, 24 h, and 48 h in air atmosphere. These annealing temperatures have been selected to cover the working temperature of YSZ lambda sensors. In our previous study, it was shown that addition of alumina into YSZ leads to appearance of t′ metastable phases in the grain boundaries of sintered YSZ. Considering the operating temperature of oxygen sensors (800–1000 °C), investigation on the phase transformations and structural changes of YSZ after heat treatment at those mentioned temperatures is a must.

3. Results and discussion

3.1. Electron microscopy

Fig. 2(a) represents the morphology of the YSZ material, obtained by SEM revealing a porous structure with a grain size around 400 nm. Since alumina concentration is beyond the solubility limit of YSZ, alumina particles are expected to segregate in YSZ matrix. However, there is no clue for existence of alumina segregated particles in SEM image. Fig. 2(b) shows the TEM bright field image of YSZ sample. Alumina (shiny particles) is precipitated in the YSZ matrix which led to the formation of a glassy-like phase. This image simply confirms the segregation of alumina particles between YSZ grains. Fig. 2(c) corresponds to a triple grain boundary between two YSZ (1 0 1) grains and an alumina one. Without considering the Moire fringe which appeared in the grain boundary of YSZ and alumina, apparently a second phase raised up in the grain boundary between YSZ grains. The samples contain alumina particles which are segregated in the YSZ matrix as well as alumina and yttria particles which are segregated in the grain boundaries. It is already confirmed that by adding alumina into YSZ, the grain boundary structure becomes a mixture of tetragonal, cubic, and metastable t′ phases whereas grain structure is mostly formed by tetragonal and cubic.

3.2. Thermodiffractometry of the YSZ

Fig. 3 depicts the thermodiffractometry of the as-received sintered YSZ powder at different temperatures. Temperature elevation process was done in vacuum environment, as shown in Fig. 3(a). XRD measurements were performed at room temperature in order to compare the structural variation with temperature. Since all XRD diffractions at room temperature are perfectly identical, it can be concluded that there is no structural variation during the thermodiffractometry. Diffraction peaks were indexed and corresponding phases were identified in order to detect the main phases which are presented in YSZ samples [17,18].

As shown in Fig. 3(b), by increasing the temperature, no significant change in crystallographic direction of the YSZ is seen. Fig. 1 discloses the fact that above 2000 °C cubic phase is the dominant phase. At temperatures lower than 400 °C, YSZ should be a mixture of monoclinic and cubic phases. However, even at 100 °C and 400 °C, no monoclinic phase was observed. Moreover, alumina diffraction peaks were detected with low intensities. Presence of (4 0 0) crystal diffraction at 2θ of 74° confirms the existence of cubic phase [18]. Therefore, Fig. 3(b) shows that YSZ is structured by stable and metastable tetragonal phase and cubic phase.

Fig. 3(c) illustrates the coexistence of metastable t′ and cubic phases. In our previous study, it was shown that addition of alumina into YSZ leads to the generation of t′ phases in the grain boundaries of sintered YSZ. However, the grains of sintered YSZ are mostly constructed by tetragonal and cubic phases. Hence, transformation toughening may happen at the YSZ grains when YSZ exposed to

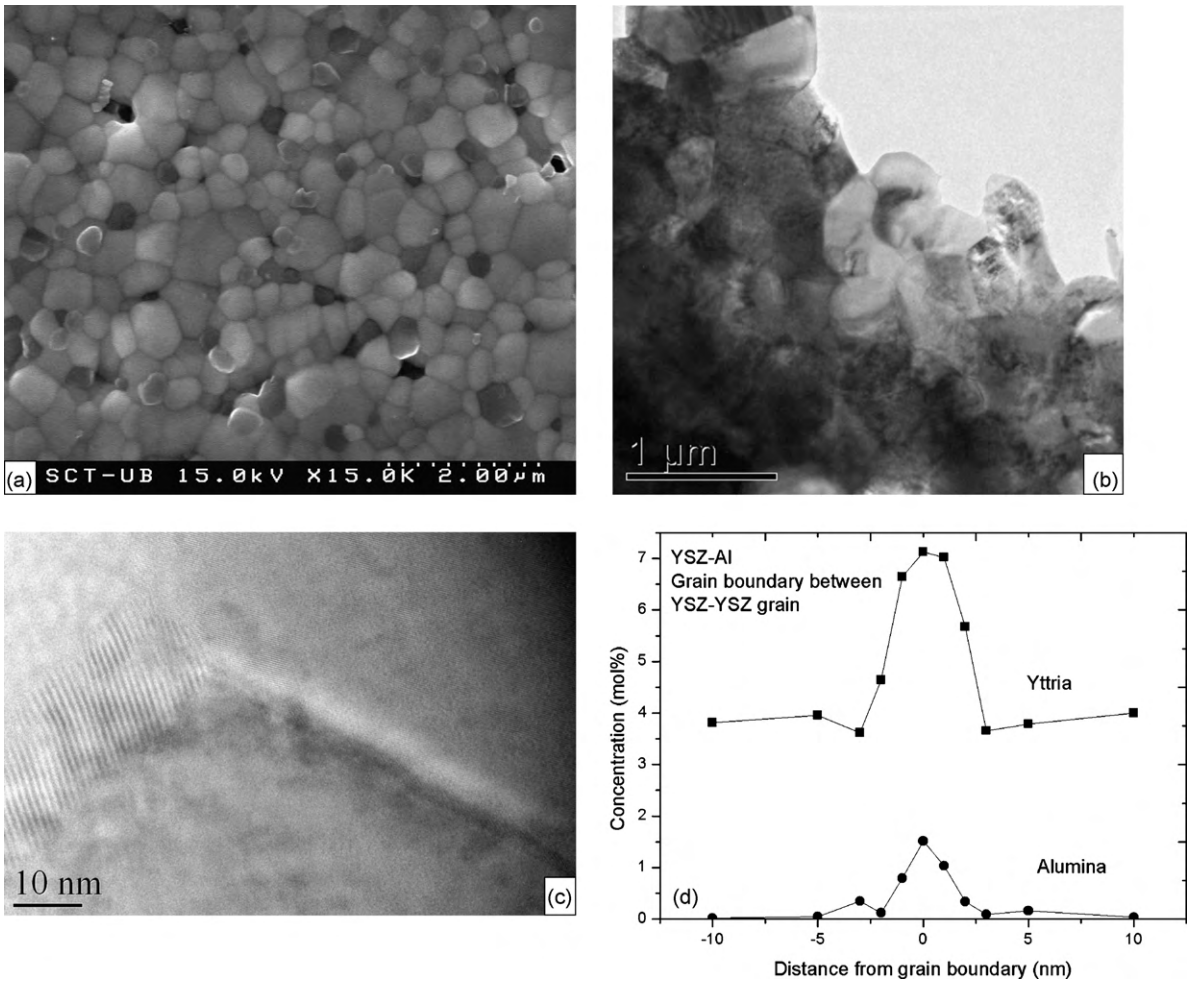

Fig. 2. SEM image of the YSZ doped with alumina shows the grain size variation (a). Segregated alumina (shiny particles) was detected by TEM image (b), HRTEM image of the grain boundaries between two YSZ grain and an alumina segregated grain (c). Second phase in the grain boundary was detected.

high temperatures for long period of time. No martensitic phase was detected for short annealing time (50 h).

3.3. Heat treatment of YSZ

3.3.1. Lattice variation

Sintered YSZ specimens were annealed at 800 °C and 1000 °C for 1 h, 6 h, 24 h, and 48 h in air to simulate working temperature of YSZ-based gas sensors. As it was already indicated in Fig. 1, above 2000 °C, cubic phase is the dominant while at temperature between 800 °C and 1000 °C, YSZ would be a mixture of tetragonal and cubic phases. Therefore, any segregation of yttria and/or alumina might be possible.

On one hand, the driving force for segregation of Y^{3+} ions in YSZ has been discussed previously from the view point of elastic energy relaxation [19] and electric neutrality at the grain boundaries [20]. On the other hand, Matsui et al. [21] proved the segregation of Y^{3+} along the grain boundaries leading to appearance of cubic phase inside the tetragonal grains along with the grain boundaries. Calculation of the lattice parameters based on XRD patterns is an effective way to detect any probable segregation. In fact, any segregation of yttria and/or alumina decreases the lattice size and the lattice parameter merges to pure zirconia lattice parameter, assuming that the generated stress because of particle segregation is negligible. Therefore, lattice parameters were measured from d-spacing of (1 0 1) and (1 1 0) crystallographic planes by means of Bragg's law for tetragonal lattice. As it is shown in Table 1, *a* and *c* parameters of the lattice relatively reduced after annealing at 800 °C and 1000 °C whereas tetragonality remains constant. Viazzi et al. [18] presented the relation between the domain stability of different tetragonal forms of YSZ and the ratio of their cell parameters. By considering the limited solubility of alumina in zirconia, YSZ samples are positioned in the transformable tetragonal region. Since the grain boundaries mostly consist of t′ phase, the grain boundary structure is non-transformable. This might be the origin of desirable high temperature mechanical properties of alumina-doped YSZ.

Table 1
Lattice parameter and tetragonality variation after annealing for different times at 800 °C and 1000 °C.

	As-produced	1 h		6 h		24 h		48 h	
		1000 °C	800 °C	1000 °C	800 °C	1000 °C	800 °C	1000 °C	800 °C
a	3.6052	3.6037	3.6014	3.6034	3.5980	3.6034	3.5968	3.6015	3.5943
c	5.1882	5.1866	5.1974	5.1839	5.1903	5.1838	5.1888	5.1804	5.1887
Tetragonality	1.0177	1.0176	1.0204	1.0172	1.0200	1.0172	1.0200	1.0171	1.0207

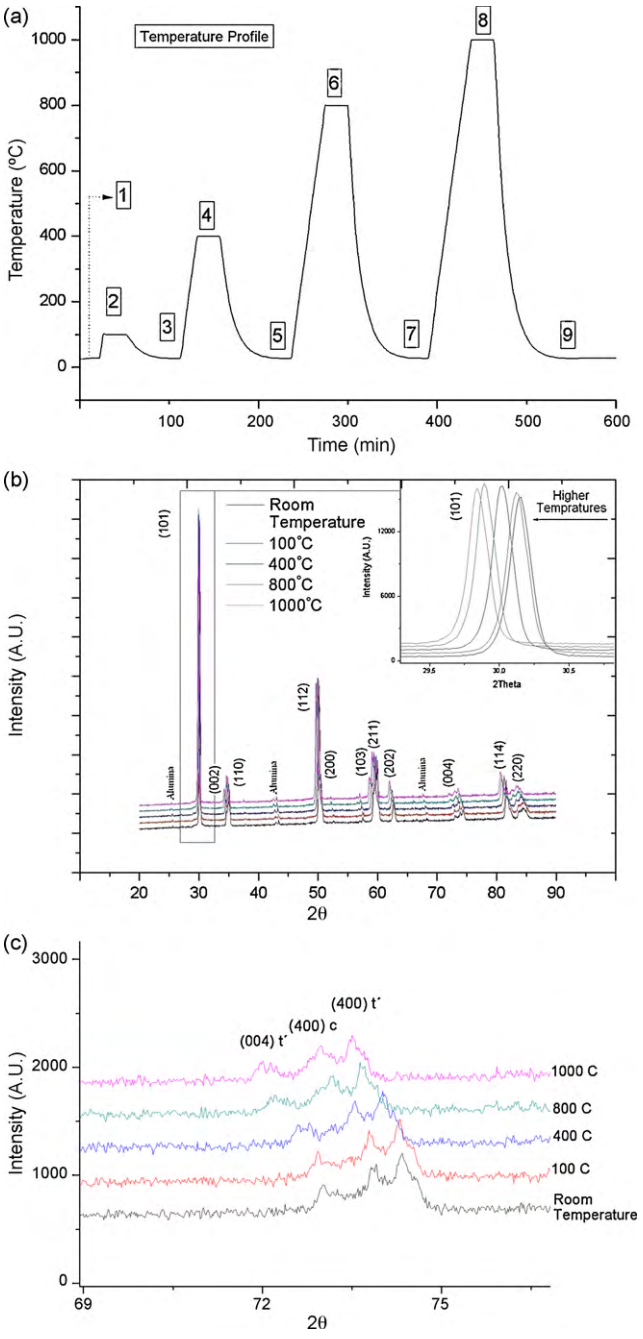

Fig. 3. In situ XRD results of oversaturated YSZ at different temperatures; temperature profile versus time (a), in situ XRD results at different temperatures (b), variation of *c* parameter and tetragonality versus temperature (c) which indicates the presence of t′ phase, and presence of cubic and t′ metastable phase (d).

SEM images of the annealed YSZ samples show that the grain size did not vary by annealing at different temperatures (Fig. 4(a)–(c)) and it is constant around 400 nm. In high temperature devices, grain size variation is definitely important due to the fact that increasing grain size causes destabilization of tetragonal phase and attendant cracking. From SEM images of Fig. 4(a)–(c), it could be concluded that grain size remains constant after annealing and therefore, phase transformation induced by grain size variation is not expected.

XRD patterns of annealed samples at 1000 °C are shown in Fig. 5. The presence of t′ phase at room temperature is significant while there is no evidence of monoclinic phase. Apparently, the peak corresponding to (4 0 0) plane of cubic phase is disappeared. However,

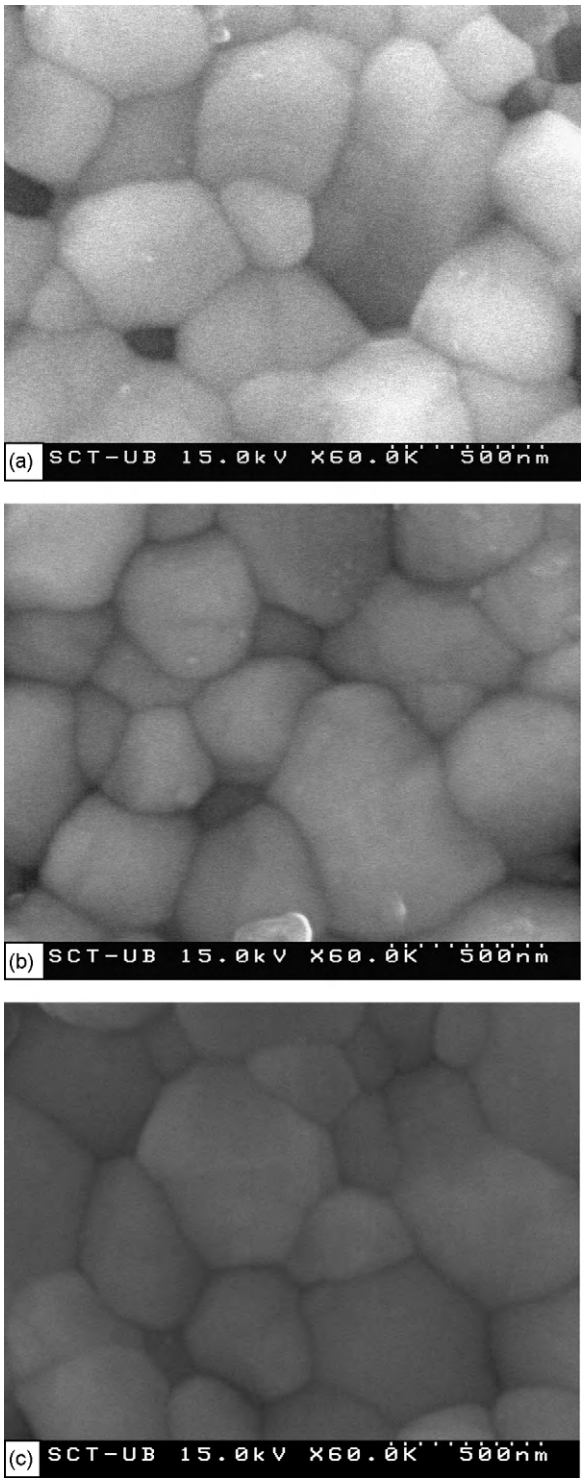

Fig. 4. SEM images of the sintered YSZ doped with alumina after annealing at 800 °C for 24 h (a) and at 1000 °C for 6 h (b) and 48 h (c). Grain growth has not been detected after heat treatment and grain size did not vary.

(2 0 2) diffraction of cubic phase still exists. One could conclude that the cubic phase is partially disappeared. Since there is no clue for existence of monoclinic phase, this cubic phase may have been transformed into tetragonal one. Segregation of yttria and/or alumina might be the reason of the mentioned transformation.

3.3.2. *Raman spectroscopy*

Raman scattering from tetragonal to monoclinic zirconia is eccentrically strong with unique spectrum, aiding identification

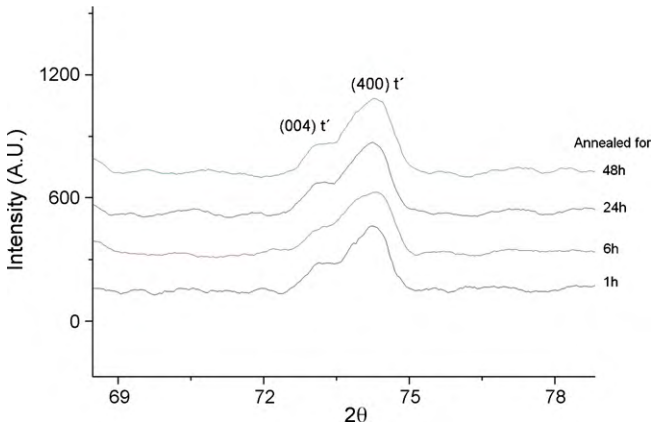

Fig. 5. XRD results showing the presence of t′ metastable phase at room temperature after annealing and cooling process.

of complex systems containing many different materials [22]. As shown in Fig. 6(a), Raman spectra of the annealed sample at 1000 °C showed the tetragonal symmetry which has six active modes only. However, no evidence of monoclinic phase is observed which is in agreement with the XRD results. It can be seen that the center positions of high intense band at 260 cm^{-1} has been shifted after annealing. However, Raman spectra are quite similar for different annealing times at 1000 °C, illustrating the difference between annealed and as-received samples (Fig. 6(b)). Additionally, the full width at half maximum (FWHM) of the band at 260 cm^{-1} became narrower after annealing at 1000 °C. Lughi and Clarke [23] showed the Raman spectra of the 5 wt% yttria-stablized zirconia at high temperatures. They indicated six band characteristics of tetragonal zirconia throughout the temperature range until 1100 °C with all the bands broadened and shifted toward lower wave number by increasing the temperature. They proved that the observed shift can be attributed to volumetric contribution due to the piezospectroscopic shift associated with the thermal expansion of the material. Hence, the shift of the Raman spectra to the higher wave numbers after annealing might be due to a decrease in the lattice dimensions. This is in agreement with the variation of *a* and *c* lattice parameters obtained by XRD (Table 1). It is noteworthy that the intensity ratio I_4/I_6 (Fig. 6(c)) increased for longer annealing times at 800 °C. It has been found previously that with increasing the Y_2O_3 concentration, the intensity ratio (I_4/I_6) decreases. This explains the lower oxygen displacement at higher concentrations of Y_2O_3 [4]. The variation of I_4/I_6 ratio could be due to the deficiency of yttria and/or alumina in YSZ. This deficiency may arise because of the segregation of dopants within the grain boundaries. Considering the fact that alumina solubility in zirconia is limited, its segregation would be negligible. Hence, yttria may partly migrate from cubic YSZ toward grain boundaries which may theoretically lead to transformation of cubic to tetragonal phase.

3.3.3. Grain boundary composition of YSZ after thermal treatment

Fig. 7 presents the grain boundary composition of yttria and alumina measured by means of EDS nanoprobe. Fig. 7(a) and (b) corresponds to annealed YSZ at 1000 °C for 6 h and 48 h, respectively. By comparing Fig. 7(a) and (b) with part 1 of this article, it could be concluded that alumina concentration did not vary after annealing at 1000 °C. However, at the same temperature, yttria concentration in grain boundaries increases for longer annealing times. Besides, yttria concentration within the grains reduces from 4 mol% to around 3 mol% (Fig. 7(b)) by annealing. This confirms the segregation of yttria after heat treatment which leads to the deficiency of yttria in YSZ. Similar phenomenon was observed after annealing at 800 °C, though the segregation rate was slower. This is due to the fact that diffusion is a thermally activated phenomenon. Therefore, it could be concluded that by long time annealing at high temperature, cubic phase of alumina-doped YSZ transforms into tetragonal along with the possibility of monoclinic phase formation. In addition, grain boundaries become slightly wider (from 4–5 nm to 5–6 nm) after segregation of yttria.

3.3.4. Hardness and mechanical properties

The Vickers microhardness (HV) was deduced from the diagonal length (2*a*) of the indentation print and the contact load (*P*) by the

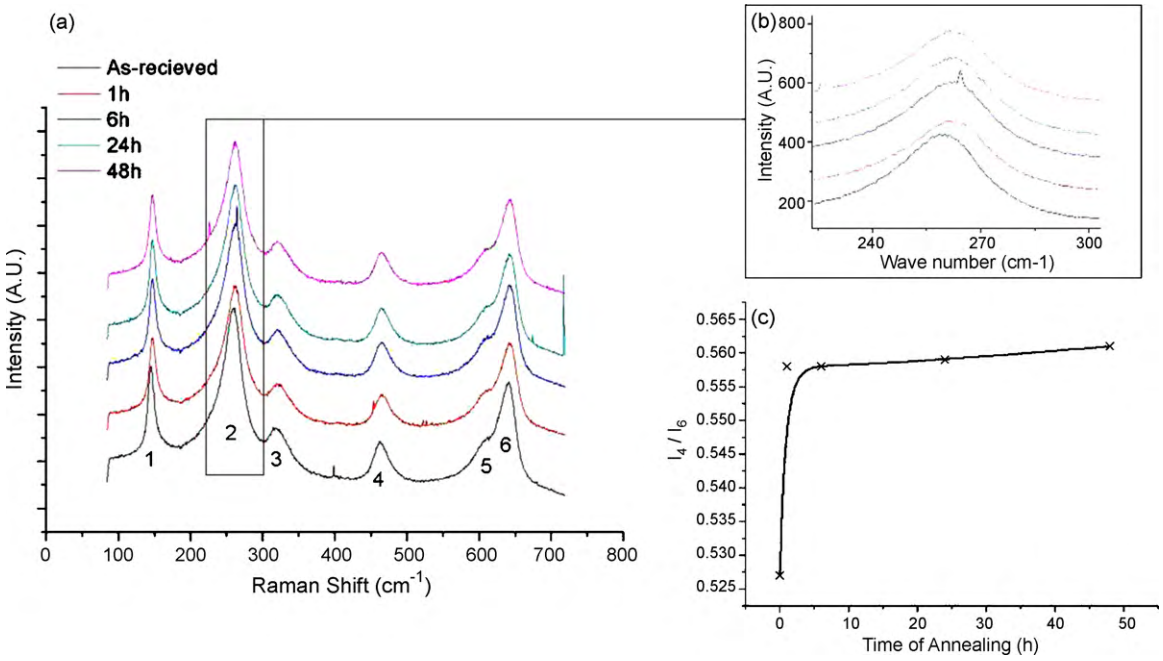

Fig. 6. Raman spectra for different annealing times at 800 °C (a), magnified main active mode (b), and variation of I_4/I_6 versus time of annealing at 800 °C (c).

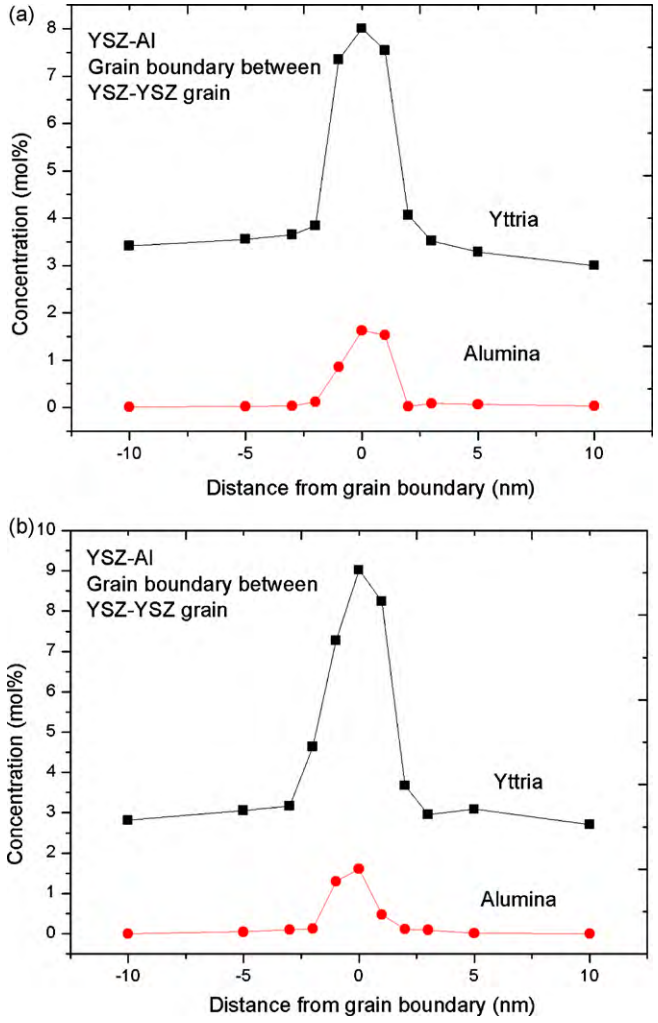

Fig. 7. Yttria and alumina concentration profile in the YSZ–YSZ grain boundary after annealing at 1000 °C for 6 h (a) and 48 h (b).

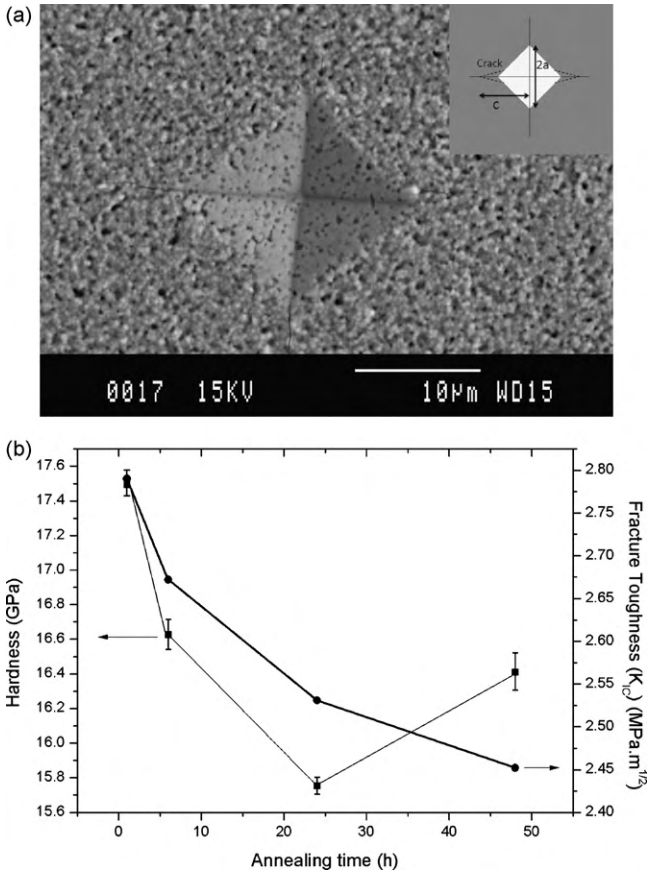

Fig. 8. SEM image of indentation area by hardness test of the YSZ doped with alumina after annealing at 800 °C for 6 h (a), the parameters to measure hardness and fracture toughness were schematically shown in top right image of (a). Variation of hardness and fracture toughness versus annealing time at 800 °C were presented in (b). The average hardness was considered for fracture toughness measurement.

following equation [24]:

$$\mathrm{HV} = 1.854\frac{P}{(2a)^2} \quad (1)$$

For fracture toughness (K_{IC}) calculations, a maximum load of 10 N was used in order to produce cracks. The average crack length (c) was measured with SEM images (Fig. 8(a)). The distance between indents was selected to be of the order of 2 mm. K_{IC} was derived from the equation proposed by Anstis et al. [25] for half-penny cracks:

$$K_{IC} = 0.0154\left(\frac{E}{\mathrm{HV}}\right)^{1/2}\frac{P}{C^{3/2}} \quad (2)$$

where E is the elastic modulus of the material, which is assumed to be constant after annealing the samples.

Fig. 8(b) presents the variation of hardness and fracture toughness after heat treatment at 800 °C for different annealing times. It can be seen that hardness decreases until 24 h of annealing while it increases afterwards. Surprisingly, this variation is in agreement with variation of tetragonality obtained by XRD (Table 1). It can be suggested that as much yttria goes out of the lattice, the hardness value becomes smaller. However, there is no clear reason for further increase of hardness and tetragonality after long time annealing (>24 h). One possible explanation is, since YSZ is oversaturated with alumina, alumina may diffuse in the octahedral sites of the lattice and compensate the deficiency of yttria in the lattice partially. This results in an increase in the tetragonality and hardness as well. However, there is no clue about the onset of this compensation (24 h annealing) and about the continuing of this trend for longer annealing times. Besides, high porosity of the YSZ may affect upon the accuracy of the hardness measurement as well.

Moreover, fracture toughness reduces by increasing the annealing time. This means that the ability of YSZ which contains cracks to resist against fracture is decreased. Mathematically, fracture toughness slope is getting horizontal at higher annealing time. Particularly for 48 h annealing, increase in the hardness has been compensated by higher crack length. Higher crack length represents brittleness of the annealed sample at higher annealing time. A possible explanation is the segregation of yttria toward the grain boundaries of YSZ. This segregation essentially introduces stacking faults and dislocation around the grain boundaries which makes YSZ more brittle.

3.4. Impedance spectroscopy at different temperatures

Fig. 9 shows the typical impedance curves of YSZ at different temperatures in order to identify the effect of thermal cycles on the resistance of YSZ as electrolyte. Measurements were carried out with two platinum electrodes deposited on YSZ which may bring redundant overlapping in the electrode impedance loop. However, as electrolyte resistance has been intended, it is reasonable to waive the overlapping effects. This experiment was designed to simulate temperature variation of YSZ gas sensor in the engine. YSZ heated up not beyond 950 °C due to the fact that nominal temperature of

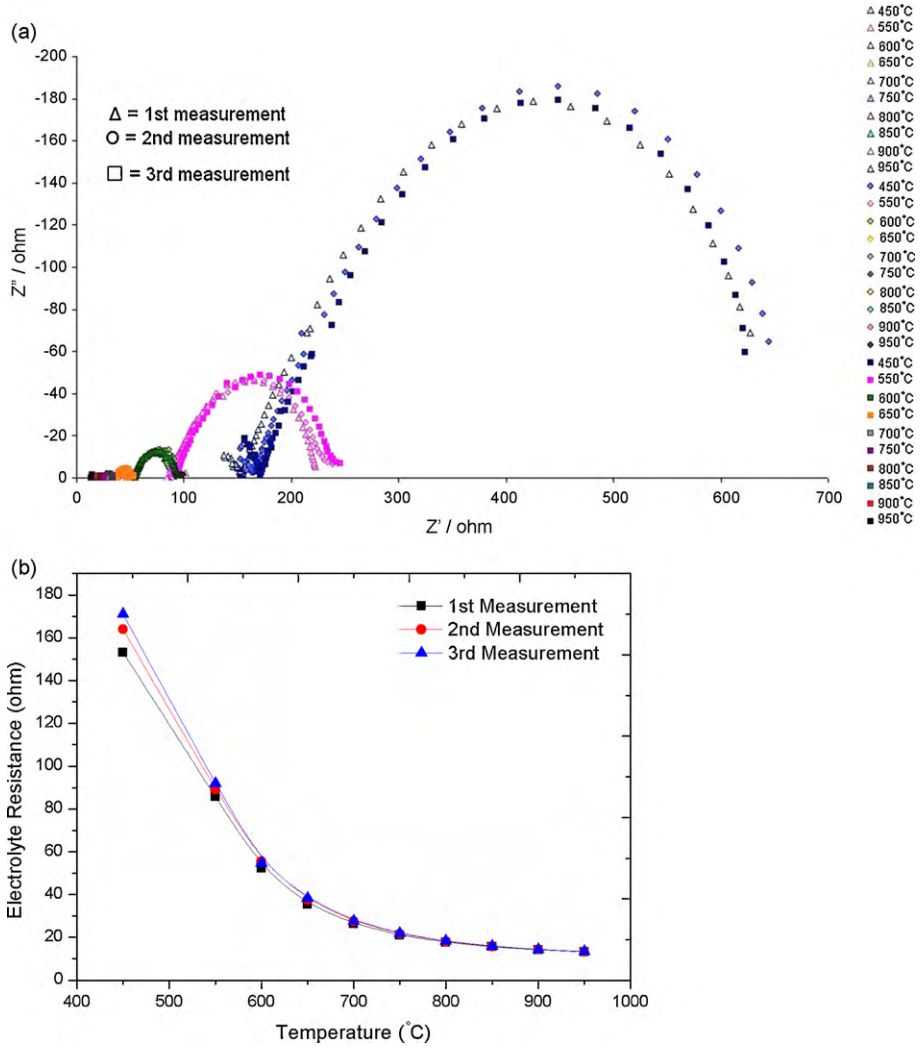

Fig. 9. Impedance spectra of sintered YSZ doped with alumina at different temperatures (a), and the plot of YSZ resistivity versus temperature (b).

the YSZ-based gas sensors does not exceed 1000 °C. Besides, the minimum temperature of sensor functionality was set to be 450 °C to assess the suitable ionic conductivity. The experiment was performed in three cycles during which YSZ heated up from 450 °C to 950 °C and then cooled down in air atmosphere. Impedance spectroscopy has been done respectively in different temperatures from 450 °C with 50 °C temperature increment.

As shown in Fig. 8(a), it could be seen that second cycle of measurements shows electrolyte resistance higher than the initial value. Moreover, the third cycle of measurements showed also a slight increase in the electrolyte resistance. These results have been summarised in Fig. 8(b) whereas difference between plots could be detected for lower quantities. However, a significant difference could be seen around 450 °C. Higher resistance is due to segregation of yttria into the grain boundaries. After each cycle, the concentration of yttria slightly increases in the boundaries. Besides, higher concentration of yttria in the grain boundaries means yttria deficiency inYSZ grains. Therefore, ionic conductivity of the grains is reduced and resistivity is increased correspondingly. In addition, widening the grain boundaries raises the resistivity of the YSZ as well, as a result of space charge layers around grain boundaries [12]. By considering numerous cycles that occur during operation of the YSZ-based oxygen sensors, electrolyte resistance increases in each cycle and thus, sensor lifetime is strongly dependent on this yttria deficiency.

3.5. Real YSZ-base oxygen sensor after 50,000 h working in the engine

YSZ-based oxygen sensor was fabricated by means of tape casting and multilayer planar ceramic technologies and implemented

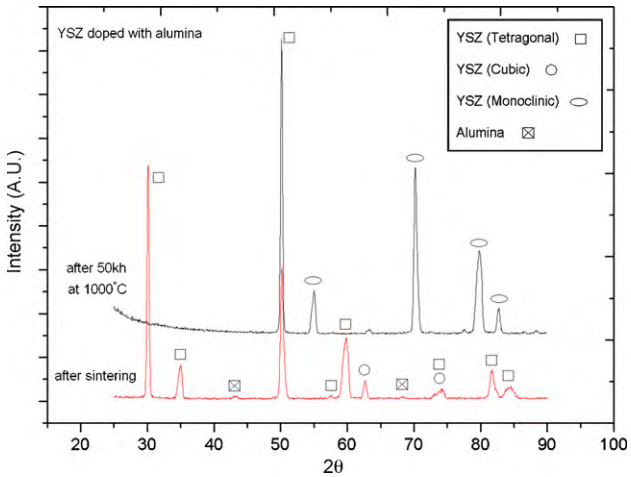

Fig. 10. XRD diffractions of YSZ doped with alumina after sintering and after 50,000 h at 1000 °C.

in the engine to work in real ambient. The fabrication process and experimental design is already described [13]. Fig. 10 depicts to XRD results of YSZ electrolyte after 50,000 h working in the engine. The examined area is far away from electrodes and is a part of the sensor's body. It can be seen that after long time exposure to high temperature and realistic conditions, cubic phases disappeared and monoclinic diffractions appeared in the XRD patterns. This confirms the vital effect of yttria segregation upon sensor lifetime. Although life time of this sensor is extremely longer than commercially available sensors, further study is necessary to enhance this property.

4. Conclusions

In conclusion, segregation of yttria in YSZ doped with alumina was detected by various characterization methods. Yttria concentration decreases in the YSZ grains as a result of annealing at 1000 °C. Although after annealing (50 h), the main phases in the samples were tetragonal and cubic, very long annealing time (50,000 h) resulted in the transformation of cubic and/or tetragonal phase to monoclinic phase due to the yttria deficiency in the structure. Besides, segregation of yttria brings about widening of the grain boundaries which may increase the resistivity of YSZ. Furthermore, segregated alumina was detected in the as-received YSZ. However, there is no clue for further segregation of alumina even though alumina content is significant in the YSZ material. Moreover, the effect of yttria segregation on the mechanical and electrical properties of YSZ was described. To confirm the proposed effect of yttria segregation on the lifetime of YSZ-based oxygen sensor, a sensor was fabricated and implemented into the engine to work for 50,000 h in real conditions. Appearance of monoclinic phase and disappearing of the cubic phase and partly tetragonal phase confirms the proposed effect of yttria segregation upon sensor lifetime. This study reveals the importance of considering the degradation of electrolyte material in the high temperature applications of YSZ.

References

[1] R. Stevens, An Introduction to Zirconia: Zirconia and Zirconia Ceramics, Magnesium Electrum, 2nd ed., Twickenham, 1986.
[2] B. Basu, J. Vleugels, O. Van Der Biest, Mater. Sci. Eng. A 366 (2004) 338.
[3] E.H. Kisi, C.J. Howard, Key Eng. Mater. 1–36 (1998) 153–154.
[4] M. Yashima, T. Mitsuhashi, H. Takashina, M. Kakihana, T. Ikegami, M. Yoshimura, J. Am. Ceram. Soc. 78 (1995) 2225.
[5] H.G. Scott, J. Mater. Sci. 10 (1975) 1527.
[6] M. Cheng, B. Hallstedt, L.J. Gauckler, Solid State Ionics 170 (2004) 255.
[7] O. Fabrichnaya, F. Aldinger, Z. Metallkde 95 (2004) 27.
[8] M. Yashima, T. Hirose, S. Katano, Y. Suzuki, M. Kakihana, M. Yoshimura, Phys. Rev. B 51 (1995) 8018.
[9] K. Oe, K. Kikkawa, A. Kishimito, Y. Nakamura, H. Yanagida, Solid State Ionics 74 (1994) 157.
[10] I.M. Ross, W.M. Rainforth, D.W. McComb, A.J. Scott, R. Brydson, Scripta Mater. 45 (2001) 653.
[11] L. Gremillard, T. Epicier, J. Chevalier, G. Fantozzi, Acta Mater. 45 (1997) 5275.
[12] J. Maier, Ber. Bunsen-Ges. Phys. Chem. 90 (1986) 26.
[13] C. Lopez-Gandara, F.M. Ramos, A. Cirera, A. Cornet, Sens. Actuators B, doi:10.1016/j.snb.2009.04.066.
[14] F. Snijkers, A. de Wilde, S. Mullens, J. Luyten, J. Eur. Ceram. Soc. 24 (2004) 1107.
[15] Z. Wang, J. Qian, J. Cao, S. Wang, T. Wen, J. Alloys Compd. 437 (2007) 264.
[16] P. Timakul, S. Jinawath, P. Aungkavattana, Ceram. Int. 34 (2008) 867.
[17] M. Yashima, S. Sasaki, M. Kakihana, Y. Yamaguchi, H. Arashi, M. Yoshimura, Acta Crystallogr. Sect. B: Struct. Sci. 50 (1994) 663.
[18] C. Viazzi, J.P. Bonino, F. Ansart, A. Barnabe, J. Alloys Compd. 452 (2008) 377.
[19] P. Thavorniti, Y. Ikuhara, T. Sakuma, J. Am. Ceram. Soc. 81 (1998) 2927.
[20] N. Shibata, F. Oba, T. Yamamoto, Y. Ikuhara, Philos. Magn. 84 (2004) 2381.
[21] K. Matsui, H. Yoshida, Y. Ikuhara, Acta Mater. 56 (2008) 1315.
[22] V. Lughi, D.R. Clarke, J. Am. Ceram. Soc. 88 (2005) 2552.
[23] V. Lughi, D.R. Clarke, J. Appl. Phys. 101 (2007) 53524.
[24] F.A. McClintock, A.S. Argon, Mechanical Behaviour of Materials, Addison-Wesley Publishing Company, Massachussets, USA, 1966.
[25] G.R. Anstis, P. Chantikul, B.R. Lawn, D.B. Marshall, J. Am. Ceram. Soc. 64 (1981) 539.